Aligning and Restoring Imperfect ssEM images for Continuity Reconstruction

Yanan Lv[1,2], Haoze Jia[1,2], Xi Chen[1(✉)], Haiyang Yan[1,3], and Hua Han[1,3(✉)]

[1] Laboratory of Brain Atlas and Brain-inspired Intelligence, Key Laboratory of Brain Cognition and Brain-inspired Intelligence Technology, Institute of Automation, Chinese Academy of Sciences, Beijing 100190, China
{xi.chen,hua.han}@ia.ac.cn

[2] School of Artificial Intellengace, University of Chinese Academy of Sciences, Beijing, China

[3] School of Future Technology, University of Chinese Academy of Sciences, Beijing 101408, China

Abstract. The serial section electron microscopy reconstruction method is commonly used in large volume reconstruction of biological tissue, but the inevitable section damage brings challenges to volume reconstruction. The section damage may result in imperfect section alignment and affect the subsequent neuron segmentation and data analysis. This paper proposes an aligning and restoring method for imperfect sections, which contributes to promoting the continuity reconstruction of biological tissues. To align imperfect sections, we improve the optical flow network to address the difficulties faced by traditional optical flow networks in handling issues related to discontinuous deformations and large displacements in the alignment of imperfect sections. Based on the deformations in different regions, the Guided Position of each coordinate point on the section is estimated to generate the Guided Field of the imperfect section. This Guided field aids the optical flow network in better handling the complex deformation and large displacement associated with the damaged area during alignment. Subsequently, the damaged region is predicted and seamlessly integrated into the aligned imperfect section images, ultimately obtaining aligned damage-free section images. Experimental results demonstrate that the proposed method effectively resolves the alignment and restoration issues of imperfect sections, achieving better alignment accuracy than existing methods and significantly improving neuron segmentation accuracy. Our code is available at https://github.com/lvyanan525/Aligning-and-Restoring-Imperfect-ssEM-images.

Keywords: image alignment · ssEM · imperfect sections.

1 Introduction

The ssEM (serial section electron microscopy) reconstruction method is crucial in volume reconstructions[13][14]. However, section damage is inevitable, especially in the reconstructions of large samples[1][7]. The inevitable section

damage may result in imperfect section alignment, subsequently affecting subsequent processes like neuron segmentation and data analysis. Therefore, aligning the imperfect section is of great significance for ssEM reconstruction. Common manifestations of section damage include cracks and folds, as shown in Fig. 1. Cracks disrupt the structure of the biological tissue, but the tissue is still largely preserved. In some cases, it is possible to restore the tissue to its pre-damaged state. However, the situation is more challenging with folds as the loss of section information is irreversible. Cracks or folds both cause structural fractures and significant deformation of biological tissue on the section. As the deformations are large and discontinuous, coupled with the loss of reference information, it becomes challenging for subsequent serial section alignment.

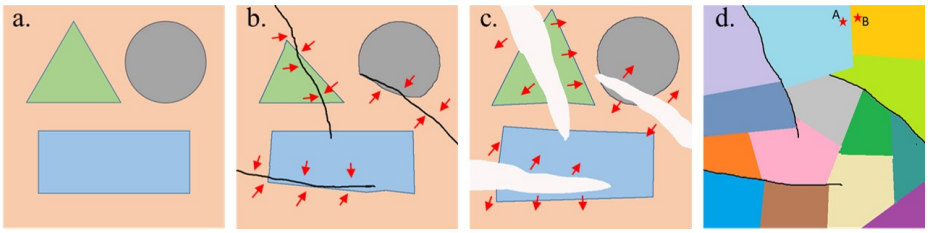

Fig. 1. diagram of common manifestations of section damage. (a) Section without damage. (b) Crack in the section. The deformation direction of the tissue near the crack is roughly indicated by the red arrow, pointing away from the crack. (c) Fold in the section. The tissues on both sides of the fold move towards the fold, as indicated by the red arrow. (d) Diagram of categories clustered by k-means clustering algorithm. Each color represents a distinct category.

The popular ssEM image alignment methods[3][5][18] mainly focus on the serial sections without damage, with little attention on imperfect sections. In recent years, large volume reconstruction has brought attention to the imperfect sections. Scheffer et al.[10] aligned imperfect sections through the triangular mesh. Huang et al.[2] presented a comprehensive process that involves simulating the generation of folds and aligning imperfect sections through an improved U-Net. These efforts mainly cover relatively simple section damage cases, making them less applicable to complex damage. For large volume reconstruction, Mitchell et al.[6] introduced the SEAMLeSS method to address alignment issues arising from discontinuous deformations caused by imperfect sections. Popovych et al.[7] proposed a divide-and-conquer approach, segmenting imperfect section images into multiple fragments. Xin et al.[16] employed K-means and K-nearest neighbors (KNN) to estimate the probability density of each cluster. While these contributions offer promising methods for aligning imperfect sections in large-volume reconstructions, they fall short in the restoration of folded regions, which may pose challenges for subsequent neural tracing and segmentation tasks.

The concept of frame interpolation[11][15][17] can also be exploited to replace imperfect sections by generating it using information from its upper and

lower sections. However, such methods often discard information preserved in the originally imperfect sections, and the generated sections may lack authenticity.

In this paper, we propose a method for aligning and restoring imperfect sections, effectively promoting the continuity reconstruction of biological tissues. Addressing the challenge of aligning complex imperfect sections, Section-Alignment module is proposed based on an optical flow network. Based on the deformations in different regions, we estimate the Guided Position of each coordinate point on the section. The Guided Positions guide the initial prediction direction of optical flow network, making it better handle complex deformations and large displacements. Furthermore, considering the discontinuity of damaged regions may contradict the inherent smoothness expectation in optical flow, the smooth constraint module of the optical flow network is refined. After alignment, we restore the damaged regions of imperfect section images, resulting in an aligned and damage-free image. Experimental results demonstrate that the proposed method effectively resolves the alignment and restoration issues of imperfect sections, achieving better alignment accuracy than existing methods and significantly improving neuron segmentation accuracy.

2 Method

The paper proposes a method for aligning and restoring imperfect ssEM (serial section electron microscopy) images to facilitate continuity reconstruction, as shown in Fig. 2a. The Section-Alignment module effectively aligns imperfect section images with the reference sections. The Section-Prediction module and the Mosaic module contribute to restoring damaged regions in imperfect sections, all contributing to yielding an aligned and damage-free image.

2.1 Section-Alignment module

In the Section-Alignment module, we improve the recently unsupervised optical flow ARFlow[4], to address the challenge of aligning imperfect section images. As shown in Fig. 2b. We introduce the Guided Position Estimation sub-module, designed to estimate the Guided position for each coordinate point on the section. This module proves crucial as it guides the prediction of the optical flow network in the subsequent step. In the meantime, we further refine the smooth constraint module of the optical flow network. This refinement aims to maintain the adaptability and robustness of the optical flow network in aligning imperfect sections, thus accommodating the unique challenges posed by non-continuous damage regions.

Guided Position Estimation sub-module. The damaged regions destroy the structural continuity in the sections, which leads to significantly different deformations in different regions. The regions near the damaged region experience substantial displacement compared to other regions, exceeding the typical searching range of commonly used optical flow networks. Consequently, the

alignment method based on optical flow networks may not work successfully. We introduce the Guided Position Estimation sub-module to estimate approximate transformations that different regions of imperfect sections are subject to. It generates potential guided positions for each pixel in the Section image, providing valuable reference information for the further optimization of the optical flow network. This module aims to enhance the adaptability of the optical flow network, enabling it to better handle the complex deformations and large displacements associated with damaged regions during alignment.

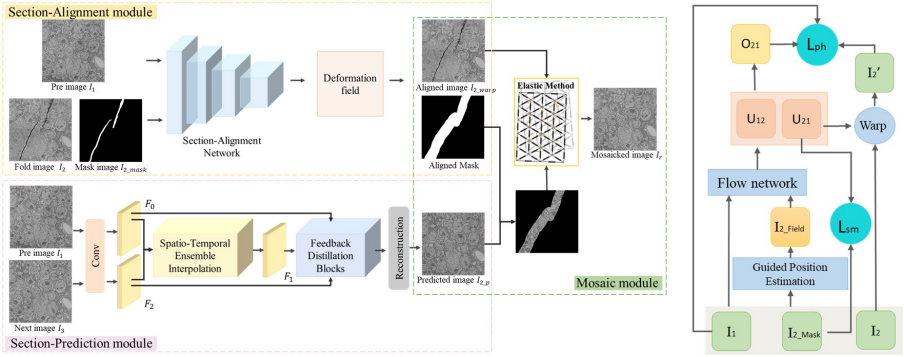

(a) pipeline of aligning and restoring imperfect ssEM images. (b) Section-Alignment module

Fig. 2. Diagram of the proposed method. (a)Pipeline of aligning and restoring imperfect ssEM images. The Section-Alignment module aligned the imperfect section I_2 with its neighboring image I_1, resulting in the aligned section image I_{2_warp}. The Section-Prediction module predicted intermediate slice I_{2_p}, by leveraging information from the neighboring sections I_1 and I_3. The Mosaic module stitched the restored image I_{2_p} of damaged regions onto the aligned imageI_{2_warp}, yielding the perfected and aligned image I_r. (b) Section-Alignment module. The Guided Position Estimation sub-module estimates the guided position for each coordinate point on the section I_2. The guided position map I_{2_field} provides guidance of the prediction of the optical flow network. U_{12} and U_{21} are the dense optical flow predicted by Flow network. $O_{12}$is the binary occlusion map, the photometric loss in the occluded region will be discarded. L_{ph} is photometric loss and L_{sm} is smooth loss.

The main idea behind the Guided Position Estimation sub-module is to divide the imperfect sections into different categories based on the deformations in different regions and apply different transformations. Regions within the same category exhibit continuous structure and are subject to similar transformations. As shown in Fig. 1d, each color represents a distinct category. Since the structure of the section except for damaged regions is continuous, it may be arbitrary to categorize regions with continuous structure, especially concerning the points near category boundaries, as marked by the red points (A and B) in Fig. 1d. This arbitrary assignment has the potential to introduce discontinuities in the regions along category borders. Instead of rigidly assigning points to specific categories,

we recalculate the probabilities of each point belonging to every category. This recalculation allows us to establish a model that considers the influence of multiple categories on each point. So, we can obtain a more accurate representation of the transformation of each coordinate point, especially the points nearing category boundaries, minimizing the risk of introducing discontinuities in the aligned image.

Assuming that the coordinate points on I_2 are clustered into k categories, denoted as $c_1, c_2, \ldots, c_k$. The transformations corresponding to each category are $T_1, T_2, \ldots, T_k$. The probability that each point p belongs to c_i is

$$\rho\left(p, c_i\right) = \frac{l_i}{\sum_{j=1}^{k} l_k} \tag{1}$$

$$l_i = \frac{1}{d_i + \epsilon} \tag{2}$$

Where d_i is the path distance between coordinate point p and the center of c_i, ϵ is a constant close to 0 (e.g. 1e-10).

The transformation of each coordinate point is

$$T(p) = \sum_{i=1}^{k} \frac{\rho\left(p, c_i\right) T_i}{\sum_{j=1}^{k} \rho\left(p, c_j\right)} \tag{3}$$

Based on the transformation $T(p)$ of all coordinate points on the section, a guided deformation field of the imperfect section can be generated.

Smooth constraint Since the motion directions on either side of the damaged region may not only be dissimilar but also exhibit opposing trends, the traditional smooth constraint may go astray, resulting in poor alignment results.

We changed smooth loss as

$$L_{loss} = \sum_{d \in x,y} \sum_{p} \| I_m \nabla_d U \| e^{-|I_m \nabla_d I|} \tag{4}$$

Where U is the optical flow field matched to the reference image. I_m is the mask of the damaged region of moving image I after each iteration of deformation.

This smooth constraint is intended to enhance the accuracy and robustness of the alignment process in the presence of discontinuous damage.

2.2 Section-Prediction module

The Section-Prediction module was used to predict the damaged region of imperfect section based on the relationship between the neighboring upper and lower sections. It is mainly based on our previous work STDIN [12], a spatio-temporal distilled interpolation method for electron microscope images. Through the Section-Prediction module, we obtained the restored image I_{2_p} of imperfect section. The effectiveness of this method has been validated on publicly available data CREMI(https://cremi.org/).

2.3 Mosaic module

Due to potential misalignment, directly cropping the restored image generated by the Section-Prediction module and replacing it on the damaged region in the imperfect section may be impractical. Therefore, the Mosaic module is introduced as shown in Fig. 2a. We first crop the restored image I_{2_p} based on the mask warp with padding, denoted as I_{wm}. Then, the elastic alignment method[9] effectively mosaic I_{wm} and I_{2_warp}. The mosaic module helps seamlessly mosaic the restored section onto the damaged region in aligned images.

3 Experiments and Results

We have compared the proposed method with several alignment methods, including SiftFlow[3], ARFlow[4], SEAMLeSS[6], and EA[16]. We have evaluated the accuracy performance on aligning imperfect sections and the benefits for continuity reconstruction among the proposed method and the compared methods. The experiments are performed on two datasets: FAFB data[19] and zebrafish brain ssEM data[16], consisting of 100 pairs of images each. The resolution of images is $32nm \times 32nm$, the image size is 1024×1024 pixels. All image pairs are coarsely aligned by affine transformation in advance. All models are trained with Intel(R) Xeon(R) Gold 6142 CPU and one NVIDIA Tesla V100 GPU.

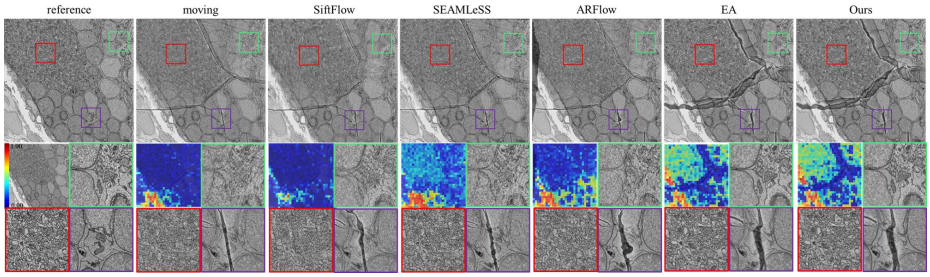

Fig. 3. The accuracy visualization result for the compared method and our method. The region in green rectangle represents regions away from folds, where ssEMnet, SEAMLeSS, and ARFlow have achieved relatively good results. The regions in red and purple rectangles depict regions close to folds, where only EA and our method have demonstrated notable effectiveness.

3.1 The accuracy performance of imperfect section Alignment

We illustrate the accuracy visualization result in Fig. 3. It also shows the alignment accuracy in different locations visually by heatmap. We overlay the alignment results of the imperfect section and the reference section image together as

the visualization result. The more artifacts in image, the less accurate the alignment is. It can be observed that our method has achieved alignment accuracy superior to the compared methods. Within areas where coarse alignment has yielded relatively commendable accuracy, both SEAMLeSS and ARFlow have demonstrated favorable alignment effects. Nevertheless, they exhibit limited effectiveness in regions that lack proper alignment during the coarse alignment. The EA method outperformed other compared methods in regions close to folds, but its alignment performance is suboptimal in certain regions.

Furthermore, we use Normalized Cross-Correlation (NCC) and Structural Similarity Index (SSIM) to evaluate the accuracy performance. As shown in Table 1, our method achieves the highest accuracy.

Table 1. Alignment accuracy comparison by Normalized Cross-Correlation (NCC) and Structural Similarity Index (SSIM)

Method	Fold(NCC)	Fold(SSIM)	Crack(NCC)	Crack(SSIM)
Moving	0.6474	0.1869	0.7385	0.3699
SiftFlow[3]	0.5901	0.0860	0.6768	0.2012
SEAMLeSS[6]	0.7512	0.4052	0.7990	0.4952
ARFlow[4]	0.7247	0.3393	0.8601	0.5974
EA[16]	0.7711	0.4167	0.8883	0.6163
Ours	**0.7830**	**0.4414**	**0.8961**	**0.6424**

Table 2. The average width (pixels) of misalignment region.

	Moving(Affine)	SiftFlow[3]	SEAMLeSS[6]	ARFlow[4]	EA[16]	Ours
Fold	150	100	140	130	90	**80**
Crack	180	150	180	120	**30**	**30**

In addition, we also compare the average width of misalignment region[7] around damaged regions. As shown in Table 2. Compared to coarse (affine) alignment, SiftFlow worsens the results. SEAMLeSS, ARFlow and EA contribute to an enhancement in alignment accuracy to varying degrees. Notably, our method achieves the highest alignment accuracy.

3.2 The benefits for continuity reconstruction

The damaged regions may disrupt the continuous of structure, which may make challenges for subsequent neuron segmentation tasks. We conducted experiments on two damaged regions with different-sized structures on the publicly available FAFB dataset, which is already well aligned. We use Section-Prediction module

and the Mosaic module to restore the damaged region, as shown in Fig. 4. U-net[8] is used to perform segmentation. The proposed method shows that the restored sections perform better segmentation than the unrestored sections.

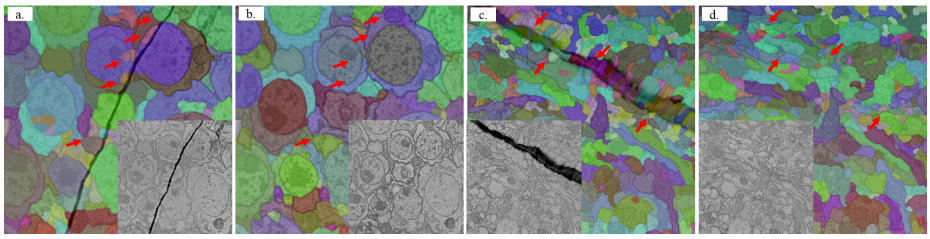

Fig. 4. The segmentation performed on restored sections and unrestored sections. (b) and (d) are the restored sections of sections (a) and (c). The red arrows mark the location where the continuity of segmentation is disrupted near the folded area. The restored sections shows better segmentation performance than the unrestored sections.

Imperfect sections may result in misalignment, inevitably affecting neuron tracing and consequently impacting the continuity reconstruction. We select 64 serial sections for experiment, in which the 32nd section is an imperfect section. We manually tracked two blood vessels (labeled as red and blue) distributed on both sides of the damaged region, as shown in Fig. 5. It is evident that there is a discontinuity observed near the damaged region due to the affine alignment method, and our method ensures the continuity of structure.

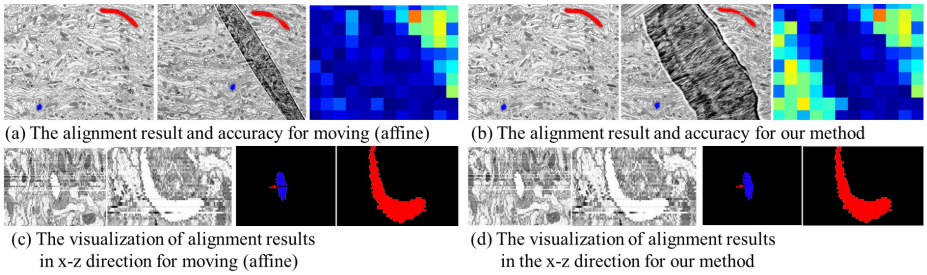

Fig. 5. The manually tracked two blood vessels distributed on both sides of the damaged region. (a) The alignment result and accuracy for affine method. The right side of the damaged region is well aligned, while the left side has lower alignment accuracy. (b) The alignment result and accuracy for our method. Both sides of the damaged region are well aligned. (c) The visualization of alignment results in x-z direction for moving (affine). The blood vessel manually tracked on the right side of the damaged region continues, while the blood vessel on the right side is discontinued. (d) The visualization of alignment results in x-z direction for our method. The blood vessels manually tracked on both sides of the damaged region are continuous.

4 Conclusion

The proposed method offers a practical solution for aligning and restoring imperfect sections, which contributes to the enhancement of alignment accuracy, promoting the continuity reconstruction of biological tissues, and the improvement of automatic segmentation precision. Experimental results demonstrate that the proposed method overtakes comparative methods in alignment accuracy, achieving the smallest misalignment area and the lowest percentage of imperfect sections. Additionally, the effective restoration of damaged regions in imperfect sections improves the accuracy of neuron tracing and segmentation, effectively promoting the continuity of neuron reconstruction.

Acknowledgments. This study were funded by STI 2030-Major Projects (2021ZD0204500, 2021ZD0204503 to L.L.), Instrument Function Development Innovation Program of Chinese Academy of Sciences (E4J92301 to Y.L.) and National Natural Science Foundation of China (No. 32171461 to H.H.).

Disclosure of Interests. The authors have no competing interests to declare that are relevant to the content of this article.

References

1. Hildebrand, D.G.C., Cicconet, M., Torres, R.M., Choi, W., Quan, T.M., Moon, J., Wetzel, A.W., Scott Champion, A., Graham, B.J., Randlett, O.: Whole-brain serial-section electron microscopy in larval zebrafish. Nature **545**(7654), 345–349 (2017)
2. Huang, W., Chen, C., Xiong, Z., Zhang, Y., Liu, D., Wu, F.: Learning to restore sstem images from deformation and corruption. In: Computer Vision–ECCV 2020 Workshops: Glasgow, UK, August 23–28, 2020, Proceedings, Part I 16. pp. 394–410. Springer (2020)
3. Liu, C., Yuen, J., Torralba, A.: Sift flow: Dense correspondence across scenes and its applications. IEEE transactions on pattern analysis and machine intelligence **33**(5), 978–994 (2010)
4. Liu, L., Zhang, J., He, R., Liu, Y., Wang, Y., Tai, Y., Luo, D., Wang, C., Li, J., Huang, F.: Learning by analogy: Reliable supervision from transformations for unsupervised optical flow estimation. In: Proceedings of the IEEE/CVF conference on computer vision and pattern recognition. pp. 6489–6498 (2020)
5. Mahalingam, G., Torres, R., Kapner, D., Trautman, E.T., Fliss, T., Seshamani, S., Perlman, E., Young, R., Kinn, S., Buchanan, J.: A scalable and modular automated pipeline for stitching of large electron microscopy datasets. Elife **11**, e76534 (2022)
6. Mitchell, E., Keselj, S., Popovych, S., Buniatyan, D., Seung, H.S.: Siamese encoding and alignment by multiscale learning with self-supervision. arXiv preprint arXiv:1904.02643 (2019)
7. Popovych, S., Bae, J.A., Seung, H.S.: Caesar: segment-wise alignment method for solving discontinuous deformations. In: 2020 IEEE 17th International Symposium on Biomedical Imaging (ISBI). pp. 1214–1218. IEEE (2020)
8. Ronneberger, O., Fischer, P., Brox, T.: U-net: Convolutional networks for biomedical image segmentation. In: Medical image computing and computer-assisted intervention–MICCAI 2015: 18th international conference, Munich, Germany, October 5-9, 2015, proceedings, part III 18. pp. 234–241. Springer (2015)

9. Saalfeld, S., Fetter, R., Cardona, A., Tomancak, P.: Elastic volume reconstruction from series of ultra-thin microscopy sections. Nature Methods **9**(7), 717–U280 (2012)
10. Scheffer, L.K., Karsh, B., Vitaladevun, S.: Automated alignment of imperfect em images for neural reconstruction. Quantitative Biology pp. abs/1304.6034, s2013 (2013)
11. Wang, Z., Liu, J., Chen, X., Li, G., Han, H.: Sparse self-attention aggregation networks for neural sequence slice interpolation. BioData Mining **14**, 1–19 (2021)
12. Wang, Z., Sun, G., Li, G., Shen, L., Zhang, L., Han, H.: Stdin: Spatio-temporal distilled interpolation for electron microscope images. Neurocomputing **505**, 188–202 (2022)
13. Winding, M., Pedigo, B.D., Barnes, C.L., Patsolic, H.G., Park, Y., Kazimiers, T., Fushiki, A., Andrade, I.V., Khandelwal, A., Valdes-Aleman, J.: The connectome of an insect brain. Science **379**(6636), eadd9330 (2023)
14. Witvliet, D., Mulcahy, B., Mitchell, J.K., Meirovitch, Y., Berger, D.R., Wu, Y., Liu, Y., Koh, W.X., Parvathala, R., Holmyard, D.: Connectomes across development reveal principles of brain maturation. Nature **596**(7871), 257–261 (2021)
15. Wu, Z., Wei, J., Yuan, W., Wang, J., Tasdizen, T.: Inter-slice image augmentation based on frame interpolation for boosting medical image segmentation accuracy. arXiv preprint arXiv:2001.11698 (2020)
16. Xin, T., Shen, L., Li, L., Chen, X., Han, H.: Expected affine: A registration method for damaged section in serial sections electron microscopy. Frontiers in Neuroinformatics **16**, 944050 (2022)
17. Yin, X.l., Liang, D.x., Wang, L., Qiu, J., Yang, Z.y., Dong, J.z., Ma, Z.y.: Analysis of coronary angiography video interpolation methods to reduce x-ray exposure frequency based on deep learning. Cardiovascular Innovations and Applications **6**(1), 17–24 (2021)
18. Yoo, I., Hildebrand, D.G., Tobin, W.F., Lee, W.C.A., Jeong, W.K.: ssemnet: Serial-section electron microscopy image registration using a spatial transformer network with learned features. In: Deep Learning in Medical Image Analysis and Multimodal Learning for Clinical Decision Support: Third International Workshop, DLMIA 2017, and 7th International Workshop, ML-CDS 2017, Held in Conjunction with MICCAI 2017, Québec City, QC, Canada, September 14, Proceedings 3. pp. 249–257. Springer (2017)
19. Zheng, Z., Lauritzen, J.S., Perlman, E., Robinson, C.G., Nichols, M., Milkie, D., Torrens, O., Price, J., Fisher, C.B., Sharifi, N., et al.: A complete electron microscopy volume of the brain of adult drosophila melanogaster. Cell **174**(3), 730–743 (2018)